Optical Continuous-Variable Qubit

Jonas S. Neergaard-Nielsen, Makoto Takeuchi, Kentaro Wakui, Hiroki Takahashi, Kazuhiro Hayasaka, Masahiro Takeoka, and Masahide Sasaki

National Institute of Information and Communications Technology (NICT), 4-2-1 Nukui-kitamachi, Koganei, Tokyo 184-8795, Japan

(Received 25 March 2010; revised manuscript received 14 May 2010; published 30 July 2010)

In a new branch of quantum computing, information is encoded into coherent states, the primary carriers of optical communication. To exploit it, quantum bits of these coherent states are needed, but it is notoriously hard to make superpositions of such continuous-variable states. We have realized the complete engineering and characterization of a qubit of two optical continuous-variable states. Using squeezed vacuum as a resource and a special photon-subtraction technique, we could with high precision prepare an arbitrary superposition of squeezed vacuum and a squeezed single photon. This could lead the way to demonstrations of coherent state quantum computing.

DOI: 10.1103/PhysRevLett.105.053602 PACS numbers: 42.50.Dv, 03.65.Wj, 03.67.−a, 42.50.Ex

Among the various physical implementation schemes of quantum-information processing (QIP), optical QIP in traveling light fields is a significant contender [1]. To avoid hard-to-implement inline nonlinearities, the linear optical quantum computing scheme (LOQC) was devised. It uses off-line resource states, linear optical processing, and photon-number resolving detection [2,3]. There are two approaches to LOQC, the standard one being the single-photon scheme, where single photons are used as the physical quantum bits (qubits) [2]. The other is referred to as coherent state quantum computing (CSQC), where two phase-opposite coherent states are used for the qubits, i.e., $|\uparrow\rangle = |\alpha\rangle$, $|\downarrow\rangle = |-\alpha\rangle$ [4–8].

CSQC is not only effective for exponential speed-up of computations, but also for attaining the ultimate capacity of an optical channel in current network infrastructure where coherent states are the primary carriers. Because coherent states propagate intact, even through lossy channels, simple coherent state encoding is found to be the optimal transmission strategy [9]. At the same time, the optimal decoding should be fully quantum, and can be implemented by an extension of CSQC [10]. Practical implementation of CSQC is still a big challenge, though—one requirement is the availability of arbitrary qubit states as resources. So far, two diagonal states of the qubit, $|\alpha\rangle \pm |-\alpha\rangle$, have been generated in the laboratories [11–16]. We will refer to these as coherent state superposition (CSS) states.

We have implemented a setup that is suited for the generation of such arbitrary qubits. For this demonstration, though, we perform the complete engineering of a different, but closely related kind of qubit, namely, one with squeezed vacuum and squeezed single-photon states as the basis. The squeezed photon state is in fact very similar to one of the CSQC diagonal qubits, as was utilized in the previous demonstrations of those. To create the arbitrary superposition of the basis states, we use single-photon subtraction from a squeezed vacuum assisted by a coherent displacement operation [17]—although in that paper it was suggested to use two-photon detection, single-photon detection allows for considerably faster data taking and still works perfectly as a demonstration of the method. Photon subtraction is a simple, but powerful technique that has been used for nonclassical state generation [11–15], entanglement increase [18,19], and fundamental tests of quantum mechanics [20] (see [21] for an overview). A related experiment for engineering of superpositions of the 0-, 1-, and 2-photon states was recently reported [22]. In our scheme, in contrast, the state elements of the superposition lie in the infinite dimensional Hilbert space, including many-photon number components.

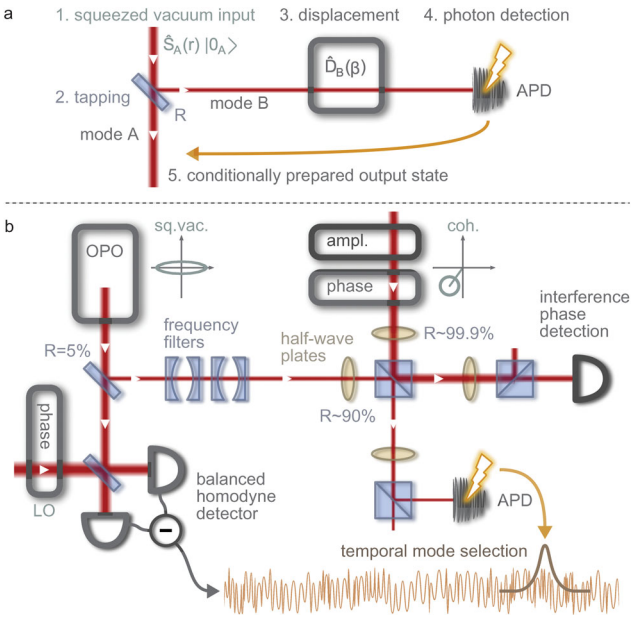

FIG. 1 (color). Experiment outline. (a) Conceptual schematic. (b) Experimental setup. OPO, optical parametric oscillator; R, beam splitter reflectivity; LO, local oscillator; APD, avalanche photodiode. See text for details.

A simplified schematic is shown in Fig. 1(a). The squeezed vacuum state $\hat{S}_A(r)|0_A\rangle$ is prepared in mode A, where $\hat{S}_A(r)$ represents the squeezing operation with strength r. A small fraction R of it is tapped off via a beam splitter as a trigger beam in mode B, subjected to the displacement operation $\hat{D}_B(\beta)$, and detected on an avalanche photodiode (APD).

The output state conditioned on an APD click is

$$\langle 1_B|\hat{D}_B(\beta)\hat{V}_{AB}\hat{S}_A(r)|0_{AB}\rangle \approx \mathcal{N}(\beta\hat{S}_A(r)|0_A\rangle - \sqrt{R}\sinh r\hat{S}_A(r)|1_A\rangle), \quad (1)$$

with normalization factor $\mathcal{N}$, and with $\hat{V}_{AB}$ representing the beam splitting operation. This superposition originates from the two indistinguishable events; an APD click comes either from the displacement or from the squeezing. In the former case the detected photon is uncorrelated with the output mode, hence leaving the squeezed vacuum state intact, $\hat{S}(r)|0\rangle$. In the latter case the output is transformed to a 1-photon subtracted squeezed vacuum state, equivalent to a squeezed photon, $\hat{S}(r)|1\rangle$. The indistinguishability of the two events leads to a coherent superposition whose weight and phase can be controlled by the parameters of the displacement operation. Each of the two states is composed of several Fock state elements—only even photon numbers for $\hat{S}(r)|0\rangle$ and odd numbers for $\hat{S}(r)|1\rangle$. They are orthogonal to each other, so together they constitute a qubit basis and the general output state (1) can therefore be represented on a Bloch sphere as

$$|\rho(\theta,\varphi)\rangle = \cos\frac{\theta}{2}\hat{S}(r)|0\rangle + e^{i\varphi}\sin\frac{\theta}{2}\hat{S}(r)|1\rangle, \quad (2)$$

with $\varphi = \pi - \arg\beta$ and, after normalization,

$$\cos\frac{\theta}{2} = \frac{|\beta|}{\sqrt{|\beta|^2 + R\sinh^2 r}} = \sqrt{\frac{n_{\mathrm{disp}}}{n_{\mathrm{disp}} + n_{\mathrm{sq}}}}, \quad (3)$$

where n_{disp} (n_{sq}) are the number of photons in mode B originating from the displacement beam (squeezing).

Our experimental setup is shown in detail in Fig. 1(b). The input squeezed vacuum states at -2.7 dB squeezing are in a cw beam generated by an optical parametric oscillator (OPO) at a center wavelength of 860 nm with a FWHM bandwidth of 9 MHz. After tapping off $R = 5\%$ for the trigger, the main part of the light (the output signal) is measured on a homodyne detector for state analysis. The trigger beam is spectrally filtered by two subsequent Fabry-Perot resonators before it is displaced and directed onto a Si APD. This filtering is required in order to avoid trigger events from nondegenerate OPO cavity modes that are uncorrelated with the homodyned mode. The phase space displacement is implemented by overlapping the beam with a weak cw coherent state on an imbalanced beam splitter [23]. Using a combination of half-wave plates (HWP) and a polarizing beam splitter (PBS), the beam splitting ratios are adjusted to experimentally convenient values. To interfere the two orthogonally polarized beams, two additional sets of HWP (45° rotation) plus PBS are needed (see Fig. 1). One output mode of the PBS is sent to the APD, while the other is monitored on a standard linear photodiode for the purpose of locking the displacement phase. The phase monitoring is done with the help of chopped probe light (10 kHz, 20% duty cycle) in both the OPO output and the displacement beam modes, and the locking is controlled by field-programmable gate array modules. Apart from this essential displacement part, the setup is mostly identical to that in Refs. [13,15], where more details are provided.

The time resolution of the trigger signal is on a scale of subnanoseconds, which is almost instantaneous compared with the ~100 ns time scale of the squeezing correlations. The trigger signal, say at time t_1, specifies a temporal mode $\psi_A(t - t_1)$ of the output state of interest, the shape and width of which are determined by the OPO output correlations [13]. In the homodyne channel, a continuous photocurrent is sampled around t_1, and subsequently integrated over $\psi_A(t - t_1)$ to yield the observed quadrature variable of the field. The specific quadrature to be measured is determined by the phase of the local oscillator (LO) of the homodyne detector. To obtain full information about the output quantum state, we must carry out many homodyne measurements at a range of different LO phases, that is, a tomographic state reconstruction. For each state, 360 000 quadrature points were observed, distributed on 12 different LO phases. The reconstruction was then done by the maximum likelihood method [24] without any correction of measurement losses.

A selection of our generated states are presented in Figs. 2 and 3. Each state is represented by its Wigner function as a top-down contour plot as well as by a Bloch sphere map of the fidelity between the state and the ideal squeezed qubit (2) for all combinations of θ and ϕ. To demonstrate the performance of the state engineering, we show in Fig. 2 the control of the superposition weight θ while keeping the phase constant at (a) $\varphi = 0°$ and (b) $\varphi = -90°$, and conversely, in Fig. 3 we show the control of the complex phase φ for fixed weights of the superposition, (a) $\theta = 135°$ and (b) $\theta = 60°$. In Fig. 2 we see that by increasing the amount of displacement in the trigger channel, $|\beta|$, we can move from the south pole (squeezed photon) to the north pole (squeezed vacuum) of the Bloch sphere along a fixed longitude. While doing that, the negative dip of the Wigner function moves away from the center in a direction determined by the displacement phase. At the same time, the dip becomes shallower and finally disappears as the state approaches the north pole. In Fig. 3, on the other hand, when sweeping the displacement phase, $\arg\beta$, the negative dip circles around the center while the state on the Bloch sphere turns around at a fixed latitude.

From the fidelity maps we can see that there is a clearly defined qubit state of maximum fidelity in the center of the

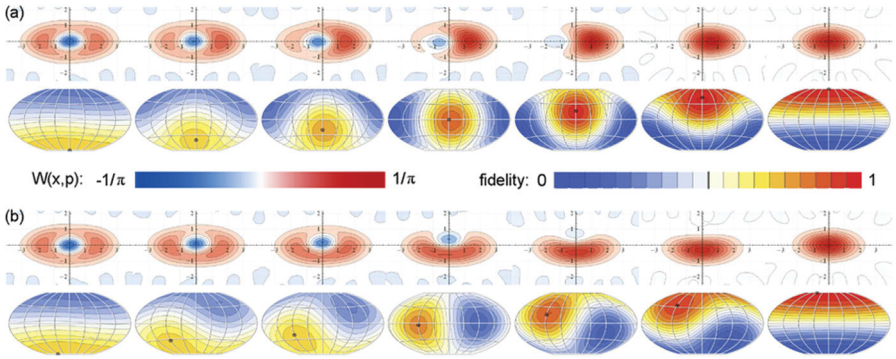

FIG. 2 (color). Control of superposition weight. A variety of experimentally generated superposition states where the superposition weight θ has been swept with the phase ϕ fixed at (a) 0° and (b) −90°. The upper panels show the Wigner function as a contour plot where the axes are the x and p quadratures. The lower panels show a flattened Bloch sphere with an overlay signifying the fidelity between an ideal qubit [Eq. (2)] at the given (θ, φ) point and the measured state. The central longitude corresponds to $\varphi = 0°$, and $\theta = 0°$ at the north pole. The small circles serve to point out which state we were aiming at. The ideal qubit is taken to have a squeezing parameter $r = 0.38$.

orange parts of the maps. These maximum points are all quite close to the target states that we aimed for in each qubit realization, marked by small circles on the fidelity maps. This illustrates the precision of our state control. It is also clear that the obtained fidelities are not as high around the south pole as they are in the north. That is because highly nonclassical states with negative Wigner functions, such as the squeezed single photon, are much more fragile and susceptible to losses than, for example, squeezed vacuum.

Equation (3) anticipates a direct correspondence between the APD click rates and the resulting superposition weight. The photon number from squeezing (displacement) is directly proportional to the count rate R_{sq} (R_{disp}) observed when blocking the displacement (trigger) beam in front of the overlapping PBS, so the relation would read $\theta = 2\tan^{-1}(R_{\mathrm{disp}}/R_{\mathrm{sq}})^{-1/2}$. This relation is shown as the green curve in Fig. 4, where also the experimentally obtained θ (of the ideal qubit with maximum fidelity) as a function of the click rate ratios $R_{\mathrm{disp}}/R_{\mathrm{sq}}$ are plotted. The data points are shown for both the $\varphi = 0°$ and the $\varphi = -90°$ series of state generation. All the points are lying below the theoretical curve. That is because the model in Eqs. (1)–(3) is an idealized picture from which there are several deviations in the actual experiment. In particular, there are unavoidable losses in state generation and measurement giving a total efficiency factor of ∼82% on the output channel. The trigger channel has an efficiency of less than 10% due to filtering, fiber coupling, low APD quantum efficiency, etc., but the effect on the output state is relatively small (it does, however, mean that the displacement coherent beam must be correspondingly weak). To more accurately describe the experimental outcomes, we have developed a relatively simple model [25] which takes into account a more detailed description of the OPO and the trigger filtering, as well as all the inefficiencies of the setup. This model, with no free parameters (except for the squeezing parameter r that is semifixed), is also plotted in Fig. 4 and is seen to simulate the measured outcomes very well. Apart from the superposition weights, the figure also shows the fidelities between the measured states and the target states—that is, the fidelity values at the target marks in the Bloch sphere maps of Fig. 2. The state preparation works somewhat better for displacement along the antisqueezing direction ($\phi = 0°$) than along the squeezing direction. This can be ascribed to the fact that losses have a larger influence on the squeezed than on the antisqueezed quadrature. The fidelities are also well described by the theoretical model, although with some smaller dis-

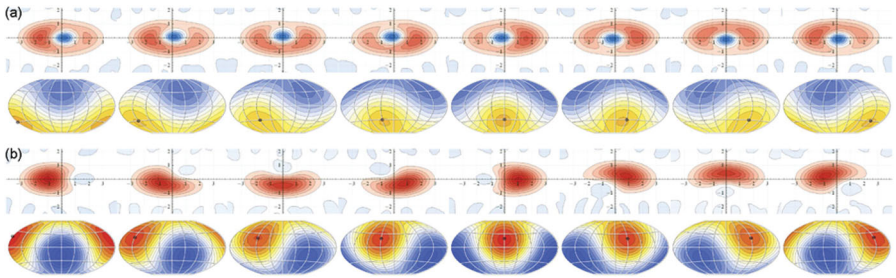

FIG. 3 (color). Control of superposition phase. Generated states with the superposition phase ϕ swept while keeping the superposition weight θ constant at (a) 135° and (b) 60°.

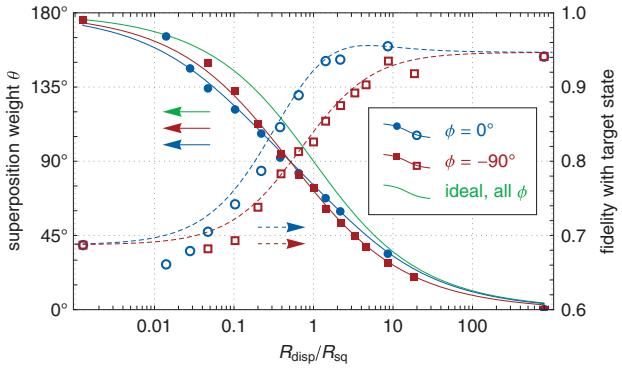

FIG. 4 (color). Influence of displacement strength. Experimentally obtained superposition weights (filled points and solid curves, left axis) and fidelities with the intended target states (unfilled points and dashed curves, right axis) versus the APD count rate of displacement photons relative to squeezing photons for two series of measurements with different superposition phase factor. The curves are obtained from a theoretical model with no free parameters. Note that the extreme data points correspond to count rate ratios of 0 and infinity.

crepancies in the weak-displacement regime. Because of the losses the states are not pure, so opposite states on the Bloch sphere are not completely orthogonal either. The qubit basis states have an overlap of 0.26, while the opposite states along the x axis and the y axis have overlaps of 0.13 and 0.25, respectively (as estimated from the model).

As these results show, we were able to realize with high precision and relatively high fidelity the complete engineering of a qubit of continuous-variable states. The simple superposition preparation technique demonstrated here can be straightforwardly applied to generation of coherent state qubits. If the input state instead of squeezed vacuum were one of the CSS states $|\alpha\rangle \pm |-\alpha\rangle$, then the single photon subtraction would change this input into the opposite state $|\alpha\rangle \mp |-\alpha\rangle$. Thus, combining this technique with the already existing CSS state [15], we should be able to generate an arbitrary superposition of these two states, equivalent to the coherent state qubits that are cornerstones of CSQC. As a side note, the currently measured basis states, squeezed vacuum and squeezed photon, already have a quite good resemblance with the "+" CSS and "−" CSS states with fidelities of 81% and 68%, respectively, for an amplitude $\alpha = 1.0$. It is also possible to generate larger amplitude CSS states by cascading the photon subtraction [26]. The results reported here can therefore lead the way to prototypes of CSQC quantum gates, likely to become important ingredients for attaining the ultimate capacity in future quantum optical networks.

We would like to acknowledge helpful discussions with Hyunseok Jeong and Chang-Woo Lee.

[1] J. L. O'Brien, A. Furusawa, and J. Vučkovíc, Nat. Photon. **3**, 687 (2009).
[2] E. Knill, R. Laflamme, and G. J. Milburn, Nature (London) **409**, 46 (2001).
[3] D. Gottesman, A. Kitaev, and J. Preskill, Phys. Rev. A **64**, 012310 (2001).
[4] P. T. Cochrane, G. J. Milburn, and W. J. Munro, Phys. Rev. A **59**, 2631 (1999).
[5] H. Jeong and M. S. Kim, Phys. Rev. A **65**, 042305 (2002).
[6] T. C. Ralph, A. Gilchrist, G. J. Milburn, W. J. Munro, and S. Glancy, Phys. Rev. A **68**, 042319 (2003).
[7] H. Jeong and T. Ralph, in *Quantum Information with Continuous Variables of Atoms and Light*, edited by N. Cerf, G. Leuchs, and E. Polzik (Imperial College Press, London, 2007), Chap. 9.
[8] A. P. Lund, T. C. Ralph, and H. L. Haselgrove, Phys. Rev. Lett. **100**, 030503 (2008).
[9] V. Giovannetti, S. Guha, S. Lloyd, L. Maccone, J. H. Shapiro, and H. P. Yuen, Phys. Rev. Lett. **92**, 027902 (2004).
[10] M. Sasaki, T. Sasaki-Usuda, M. Izutsu, and O. Hirota, Phys. Rev. A **58**, 159 (1998).
[11] A. Ourjoumtsev, R. Tualle-Brouri, J. Laurat, and P. Grangier, Science **312**, 83 (2006).
[12] J. S. Neergaard-Nielsen, B. M. Nielsen, C. Hettich, K. Mølmer, and E. S. Polzik, Phys. Rev. Lett. **97**, 083604 (2006).
[13] K. Wakui, H. Takahashi, A. Furusawa, and M. Sasaki, Opt. Express **15**, 3568 (2007).
[14] A. Ourjoumtsev, H. Jeong, R. Tualle-Brouri, and P. Grangier, Nature (London) **448**, 784 (2007).
[15] H. Takahashi, K. Wakui, S. Suzuki, M. Takeoka, K. Hayasaka, A. Furusawa, and M. Sasaki, Phys. Rev. Lett. **101**, 233605 (2008).
[16] T. Gerrits, S. Glancy, T. S. Clement, B. Calkins, A. E. Lita, A. J. Miller, A. L. Migdall, S. W. Nam, R. P. Mirin, and E. Knill, arXiv:1004.2727.
[17] M. Takeoka and M. Sasaki, Phys. Rev. A **75**, 064302 (2007).
[18] A. Ourjoumtsev, A. Dantan, R. Tualle-Brouri, and P. Grangier, Phys. Rev. Lett. **98**, 030502 (2007).
[19] H. Takahashi, J. S. Neergaard-Nielsen, M. Takeuchi, M. Takeoka, K. Hayasaka, A. Furusawa, and M. Sasaki, Nat. Photon. **4**, 178 (2010).
[20] A. Zavatta, V. Parigi, M. S. Kim, H. Jeong, and M. Bellini, Phys. Rev. Lett. **103**, 140406 (2009).
[21] M. S. Kim, J. Phys. B **41**, 133001 (2008).
[22] E. Bimbard, N. Jain, A. MacRae, and A. I. Lvovsky, Nat. Photon. **4**, 243 (2010).
[23] M. G. A. Paris, Phys. Lett. A **217**, 78 (1996).
[24] A. I. Lvovsky and M. G. Raymer, Rev. Mod. Phys. **81**, 299 (2009).
[25] M. Takeoka, J. S. Neergaard-Nielsen, M. Takeuchi, K. Wakui, H. Takahashi, K. Hayasaka, and M. Sasaki, "Photon Subtraction for Continuous Variable Quantum Information Processing" (to be published).
[26] A. E. B. Nielsen and K. Mølmer, Phys. Rev. A **76**, 043840 (2007).